atmosphere

MDPI

Article

Geomagnetic Storm Effect on F_2-Region Ionosphere during 2012 at Low- and Mid-Latitude-Latitude Stations in the Southern Hemisphere

Edwin A. Kumar and Sushil Kumar *

School of Information Technology, Engineering, Mathematics and Physics, The University of the South Pacific, Suva, Fiji; edwinkumar27@gmail.com
* Correspondence: kumar_su@usp.ac.fj

Abstract: The ionospheric effects of six intense geomagnetic storms with *Dst* index ≤ -100 nT that occurred in 2012 were studied at a low-latitude station, Darwin (Geomagnetic coordinates, 21.96° S, 202.84° E), a low-mid-latitude station, Townsville (28.95° S, 220.72° E), and a mid-latitude station, Canberra (45.65° S, 226.30° E), in the Australian Region, by analyzing the storm–time variations in the critical frequency of the F_2-region (*fo*F2). Out of six storms, a storm of 23–24 April did not produce any ionospheric effect. The storms of 30 September–3 October (minimum *Dst* = −122 nT) and 7–10 October (minimum *Dst* = −109 nT) are presented as case studies and the same analysis was done for the other four storms. The storm of 30 September–3 October, during its main phase, produced a positive ionospheric storm at all three stations with a maximum percentage increase in *fo*F2 (Δ*fo*F2%) of 45.3% at Canberra whereas during the recovery phase it produced a negative ionospheric storm at all three stations with a maximum Δ*fo*F2% of −63.5% at Canberra associated with a decrease in virtual height of the F-layer (*h'F*). The storm of 7–10 October produced a strong long-duration negative ionospheric storm associated with an increase in *h'F* during its recovery phase at all three stations with a maximum Δ*fo*F2% of −65.1% at Townsville. The negative ionospheric storms with comparatively longer duration were more pronounced in comparison to positive storms and occurred only during the recovery phase of storms. The storm main phase showed positive ionospheric storms for two storms (14–15 July and 30 September–3 October) and other three storms did not produce any ionospheric storm at the low-latitude station indicating prompt penetrating electric fields (PPEFs) associated with these storms did not propagate to the low latitude. The positive ionospheric storms during the main phase are accounted to PPEFs affecting ionospheric equatorial $\mathbf{E} \times \mathbf{B}$ drifts and traveling ionospheric disturbances due to joule heating at the high latitudes. The ionospheric effects during the recovery phase are accounted to the disturbance dynamo electric fields and overshielding electric field affecting $\mathbf{E} \times \mathbf{B}$ drifts and the storm-induced circulation from high latitudes toward low latitudes leading to changes in the natural gas composition [O/N_2] ratio.

Keywords: geomagnetic storms; prompt penetrating electric fields; disturbance dynamo electric fields; $\mathbf{E} \times \mathbf{B}$ drifts; storm-induced circulation

check for updates

Citation: Kumar, E.A.; Kumar, S. Geomagnetic Storm Effect on F_2-Region Ionosphere during 2012 at Low- and Mid-Latitude-Latitude Stations in the Southern Hemisphere. *Atmosphere* **2022**, *13*, 480. https://doi.org/10.3390/atmos13030480

Academic Editors: Christine Amory-Mazaudier and Victor I. Zakharov

Received: 23 December 2021
Accepted: 8 March 2022
Published: 15 March 2022

Publisher's Note: MDPI stays neutral with regard to jurisdictional claims in published maps and institutional affiliations.

Copyright: © 2022 by the authors. Licensee MDPI, Basel, Switzerland. This article is an open access article distributed under the terms and conditions of the Creative Commons Attribution (CC BY) license (https://creativecommons.org/licenses/by/4.0/).

1. Introduction

Geomagnetic storms are associated with space weather phenomena and strong storms can impact the whole earth's ionosphere [1–4]. The intense geomagnetic storms can cause major problems in the satellite communication and navigation systems and ground-based High Frequency communication systems (e.g., scintillations, radio blackouts) [5]. The ionospheric effect of geomagnetic storms known as an ionospheric storm varies with latitude, time of day of storm occurrence, season, and phase of the solar activity. The ionospheric effect involves complicated mechanisms including neutral winds, storm-time thermospheric composition changes and storm-generated high-latitude electric fields propagating toward

equatorial latitudes and coupling with normal ionospheric electric field [1,6–8]. The ionospheric storm is associated with changes in the ionospheric electron density (N_e) or the critical frequency of the F_2-region, *fo*F2 [9] based on which it is classified as a positive ionospheric storm (an increase in the *fo*F2 or N_e) and negative ionospheric storm (a decrease in the *fo*F2 or N_e). The ionosphere–thermosphere coupling between different latitude regions is associated with the dynamic and electrodynamic coupling from high to low latitudes and the chemical changes during the geomagnetic storms [6,8]. Sahai et al. [6] studied the effects of a major geomagnetic storm of 29–30 October 2003 at the stations, Ho Chi Minh City (10.5° N, 106.3° E), Vietnam and Okinawa (26.3° N, 127.8° E), Japan, in the East Asian sector. Authors reported both positive and negative ionospheric storms in *fo*F2 at these stations.

Storm-time perturbed high-latitude electric fields play a major contribution in the occurrence of positive and negative ionospheric storms. The perturbed electric fields during geomagnetic storms are categorized into three groups: (1) prompt penetration electric fields (PPEFs), (2) overshielding electric field, and (3) disturbance dynamo electric fields (DDEFs) [6,7,9–12]. The PPEFs are associated with the southward Z-component of the interplanetary magnetic field (IMF B_Z) and are caused by other solar wind and magnetospheric processes [8]. PPEFs are usually short-lived, around an hour [9,11] during the main phase of the storms but can exist for 6–8 h during intense geomagnetic storms [13,14]. Upon the dayside ionosphere, the southward turning of the north-south (Z) component of IMB B_z results in the eastward PPEFs and northward turning leads to the westward PPEFs. The PPEFs can cause a large enhancement in *fo*F2 or N_e in the dayside and decrease at the night side *fo*F2 or N_e [9,10,12] due to changes in the normal $\mathbf{E} \times \mathbf{B}$ drifts which are upward in the daytime and downward at the night. Overshielding electric field is associated with the northward turning of IMF B_Z when PPEFs are withdrawn towards the end of the main phase of the storm and is in the opposite direction in the dayside and nightside [12]. DDEFs are caused by the ionospheric distance dynamo effect that results from thermospheric wind circulation due to Joule heating at the high latitudes associated with geomagnetic storms. DDEFs are in opposite direction to quiet time ionospheric electric field during both day and night sides, that is, DDEFs are westward (eastward) during the dayside (nightside). The westward polarity of DDEFs reduces the *fo*F2 or N_e in the dayside and results in the contraction of equatorial ionization anomaly (EIA). On the other hand, eastward polarity reduces the F-layer downward drift at night and enhances the *fo*F2. DDEFs are slowly varying and usually long-lived. Since their arrival at the low latitudes takes about one to two days after the onset of the geomagnetic storm, their effect is dominant during the recovery phase of the storms. Researchers [6,10,15–17] have reported that the ionospheric perturbations during the recovery phase of geomagnetic storms at the mid-latitude and low latitude are mainly caused by (1) the transport of energy from high latitudes in the form of traveling ionospheric disturbances (TIDs), (2) changes in global wind pattern due to Joule heating, and (3) equatorward propagating thermospheric composition with a reduced ratio of $[O/N_2]$ gas.

In this paper, we analyzed the effects of six intense geomagnetic storms on the *fo*F2 at a low-latitude station, Darwin (Geomagnetic coordinates, 21.96° S, 202.84° E), a low-mid-latitude station, Townsville (28.95° S, 220.72° E), and a mid-latitude station, Canberra (45.65° S, 226.30° E) during 2012. These six intense storm events considered for the analysis occurred on 8–9 March (Dst_{min} = −145 nT), 23–24 April (Dst_{min} = −120 nT), 14–15 July (Dst_{min} = −139 nT), 30 September–3 October (Dst_{min} = −122 nT), 7–10 October (Dst_{min} = −109 nT), and 13–14 November (Dst_{min} = −108 nT) during 2012. An intense geomagnetic storm is defined when the minimum value of the *Dst* index falls under the criterion, -200 nT $\leq Dst \leq -100$ nT [18,19]. The peak auroral electrojet index (*AE*) and southward IMF B_Z values associated with these storms during their main phase are given in Table 1.

Table 1. Summary of the minimum value of *Dst* index and maximum value of auroral electrojet (*AE*) index and southward Z-component of interplanetary magnetic field (IMF B_Z) and its duration during the main phase of the storms. The ionospheric response during the main phase for six intense geomagnetic storms at Darwin, Townsville and Canberra stations during 2012 is also given. The detailed variation of IMF B_Z can be seen in the Supplementary Figure S1.

Storm	Min. *Dst* (nT)	Max. *AE* (nT)	IMF B_Z (nT & h)	Darwin		Townsville		Canberra	
				*fo*F2	Δ*fo*F2 (%)	*fo*F2	Δ*fo*F2 (%)	*fo*F2	Δ*fo*F2 (%)
8–9 March	−145	1785	−18.48 (~10)	No change	—	No change	—	Increase	30.0%
23–24 April	−120	1383	−15.83 (~13)	No change	—	No change	—	No change	—
14–15 July	−139	1368	−19.92 (~31)	Increase	+23.8	Increase	+25.0%	Increase	+27.4
30 September–3 October	−122	987	−20.40 (~16)	Increase	+35.7	Increase	+33.0	Increase	+45.3
7–9 October	−99 and −109	1000 and 963	−15.75 and −15.13 (~20 and 16)	No change	—	Increase	+37.6	Increase	+28.2
13–14 November	−108	1009	−17.61 (~19)	No change	—	Increase	+35.1	Increase	+40.6

2. Data and Analysis

The *fo*F2 and virtual height of F-region ($h'F$) data recorded by ionosonde during 2012 were obtained from World Data Centre, Bureau of Meteorology, Australia (online at http://www.sws.bom.gov.au/World_Data_Centre, accessed on 22 December 2021). The values of *fo*F2 available online are with scaling up by a factor of 10, and the same values were used in our plots (Figures 1–6). The disturbance storm time (*Dst*) index and *AE* index data were obtained from World Data Centre, Kyoto University, Kyoto, Japan (online at http://www.ssde.u-kigi-kyoto-ac.jp, accessed on 22 December 2021). The southward IMF B_Z values during the main phase of the storms were obtained from OMNI world data center https://omniweb.gsfc.nasa.gov/ (accessed on 22 December 2021).

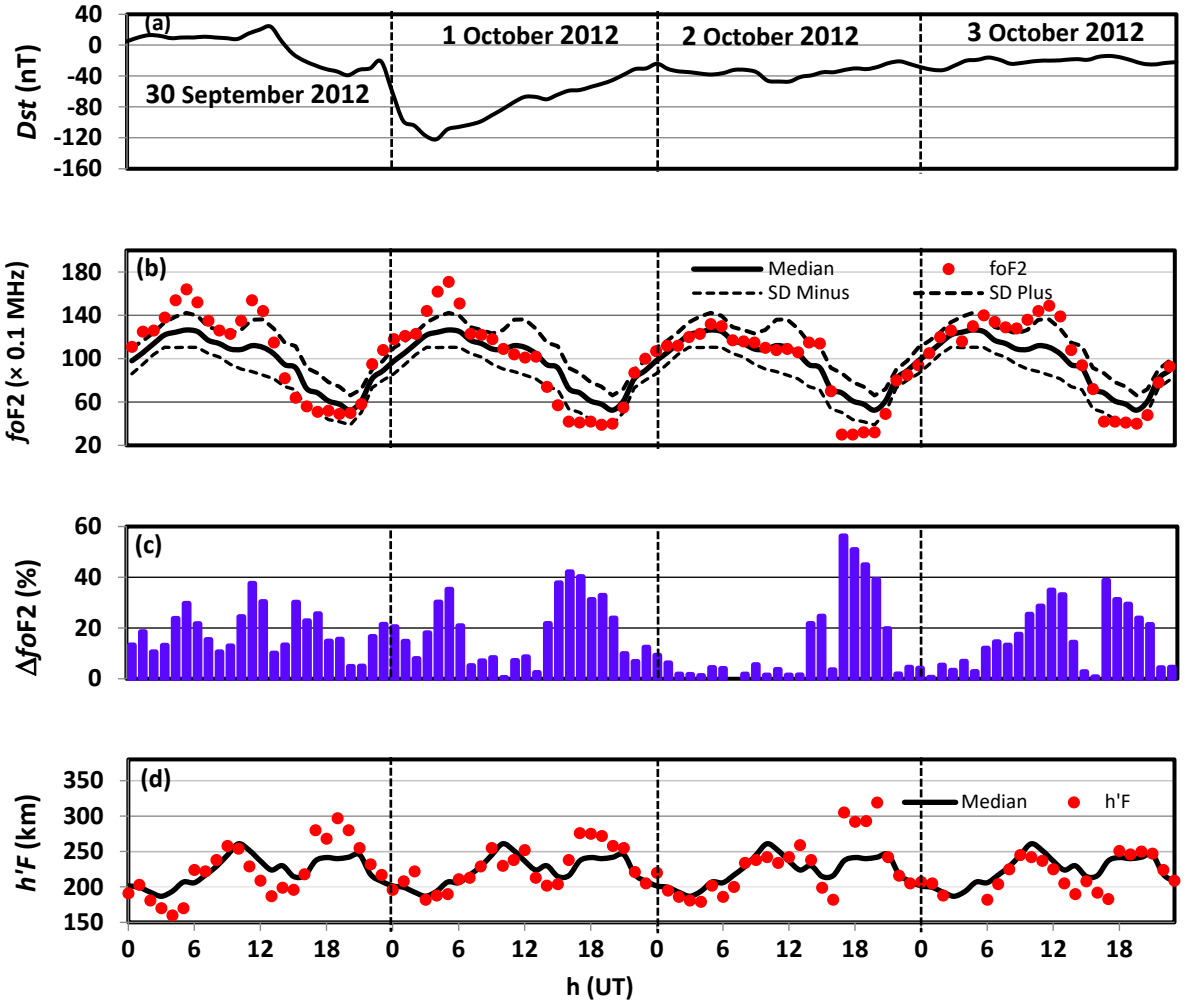

Figure 1. Variations of (**a**) *Dst* index *for* the geomagnetic storm, (**b**) hourly values of critical frequency of F_2 layer (*fo*F2) (MHz $\times$ 10^{-1}), (**c**) Δ*fo*F2%, and (**d**) virtual height of F layer ($h'F$) during 30 September–3 October 2012 at Darwin station. The median values of *fo*F2 and $h'F$ parameters are shown by solid black curves in panels (**b**,**d**). Dashed curves in panel (**b**) show the variation of *fo*F2 by $\pm$ 1 σ (standard deviation).

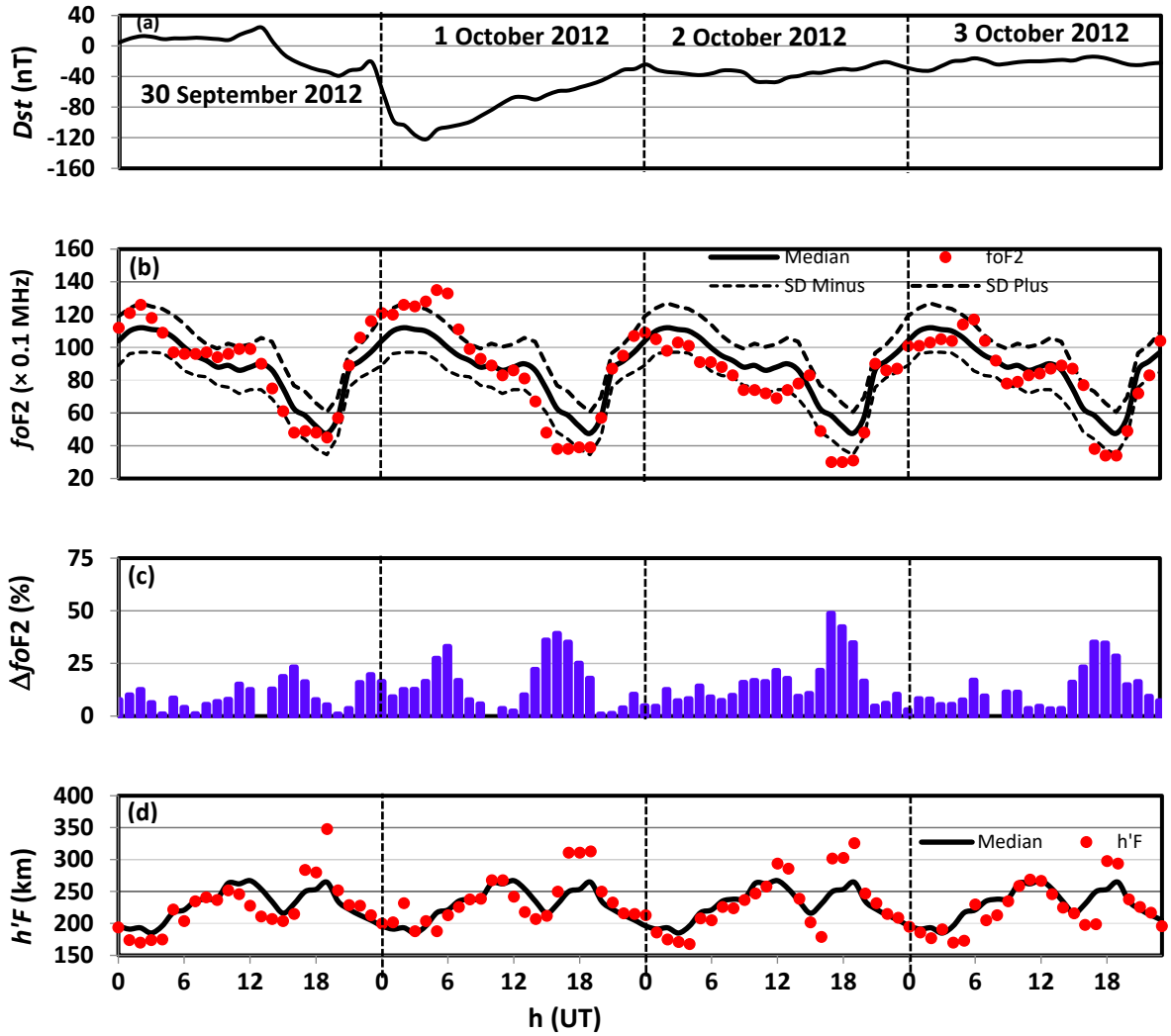

Figure 2. Variations of (**a**) *Dst* index *for* the geomagnetic storm, (**b**) hourly values of critical frequency of F_2 layer (*fo*F2) (MHz $\times$ 10^{-1}), (**c**) Δ*fo*F2%, and (**d**) virtual height of F layer ($h'F$) during 30 September–3 October 2012 at Townsville station. The median values of *fo*F2 and $h'F$ parameters are shown by solid black curves in panels (**b**,**d**). Dashed curves in panel (**b**) show the variation of *fo*F2 by $\pm$ 1 σ.

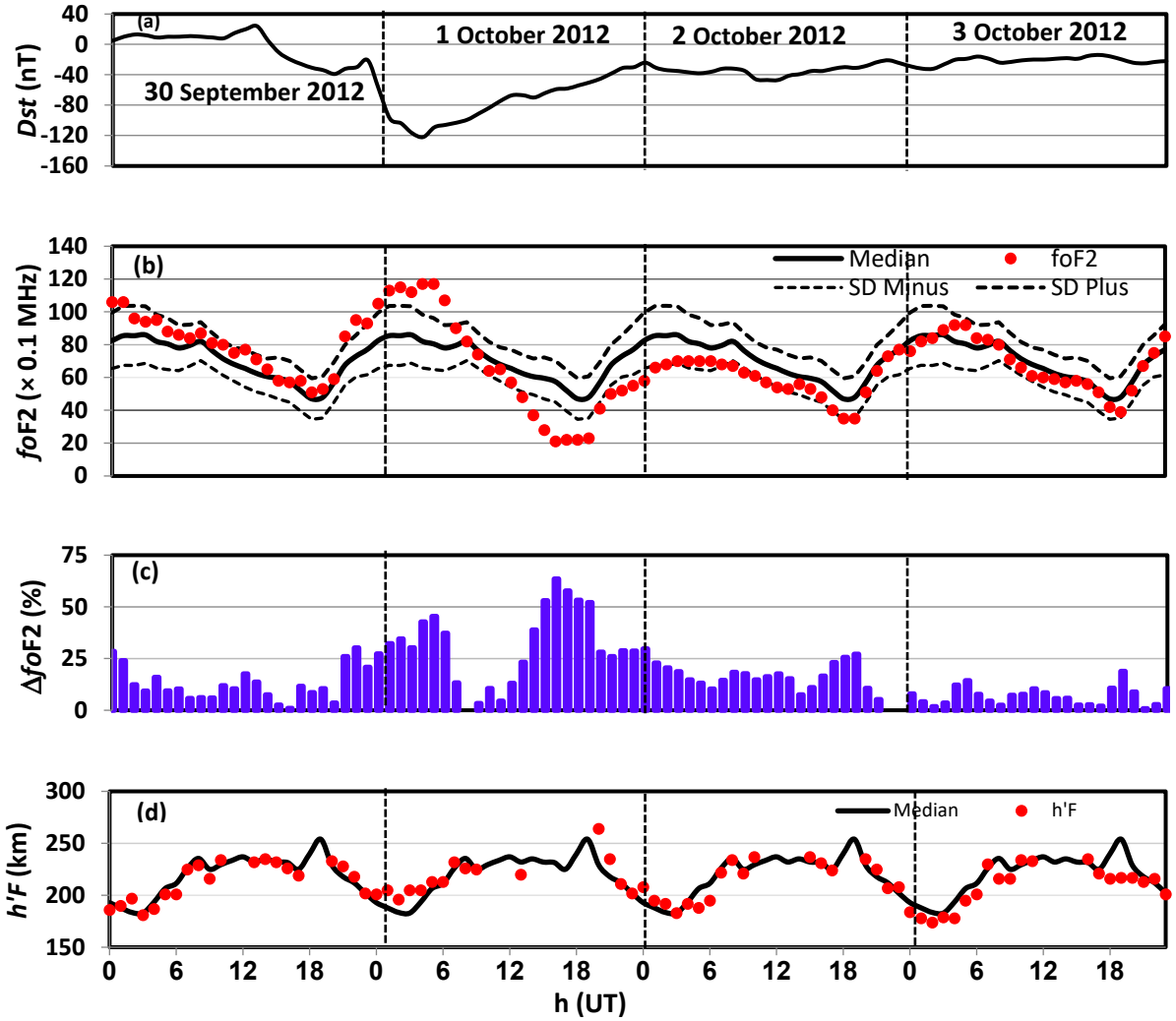

Figure 3. Variations of (**a**) *Dst* index *for* the geomagnetic storm, (**b**) hourly values of critical frequency of F_2 layer (*fo*F2) (MHz $\times$ 10^{-1}), (**c**) Δ*fo*F2%, and (**d**) virtual height of F layer ($h'F$) during 30 September–3 October 2012 at Canberra station. The median values of *fo*F2 and $h'F$ parameters are shown by solid black curves in panels (**b**,**d**). Dashed curves in panel (**b**) show the variation of *fo*F2 by $\pm$ 1 σ.

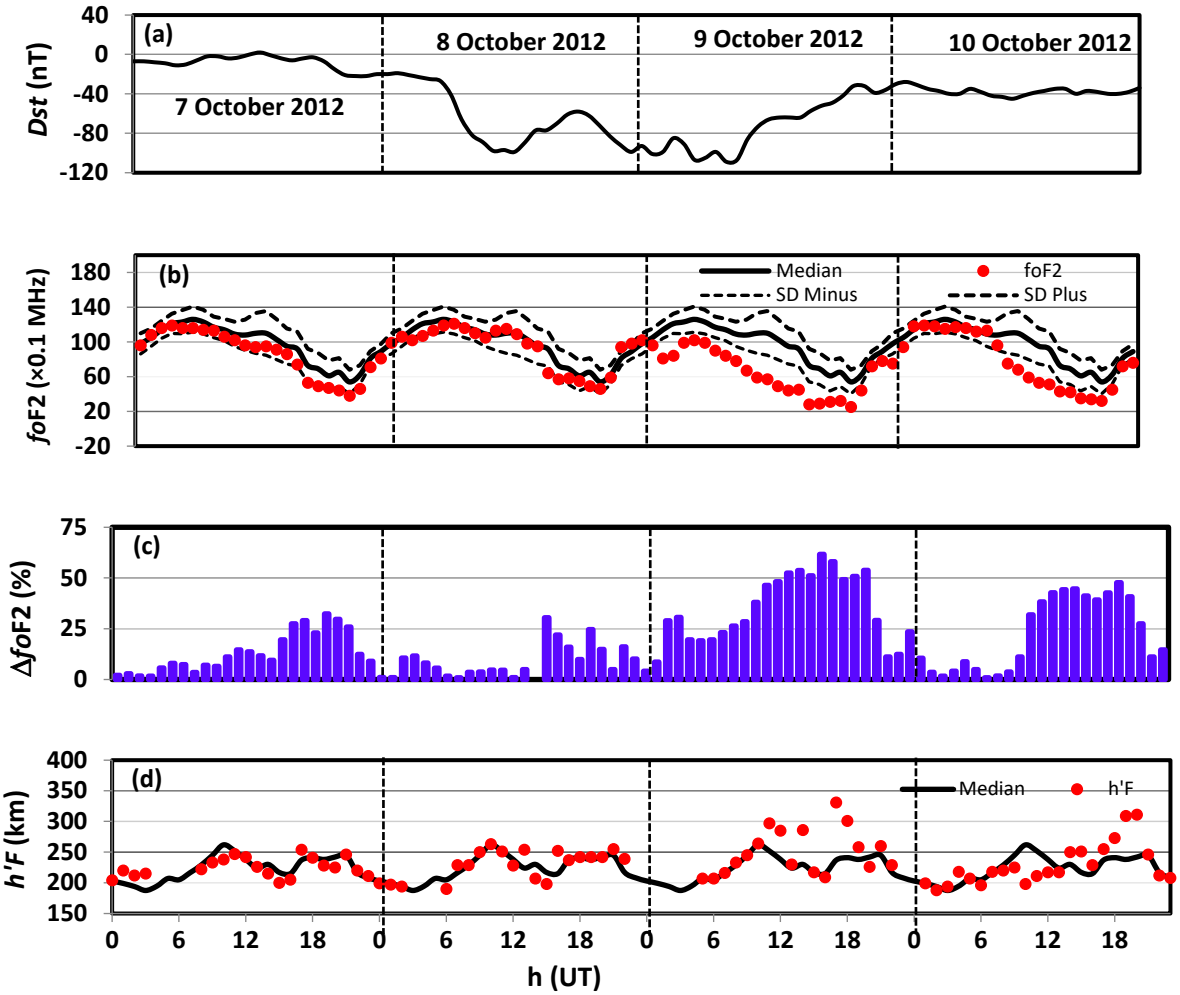

Figure 4. Variations of (**a**) *Dst* index *f*or the geomagnetic storm, (**b**) hourly values of critical frequency of F_2 layer (*fo*F2) (MHz $\times$ 10^{-1}), (**c**) Δ*fo*F2%, and (**d**) virtual height of F layer ($h'F$) during 7–10 October 2012 at Darwin station. The median values of *fo*F2 and $h'F$ parameters are shown by solid black curves in panels (**b**,**d**). Dashed curves in panel (**b**) show the variation of *fo*F2 by $\pm$ 1 σ.

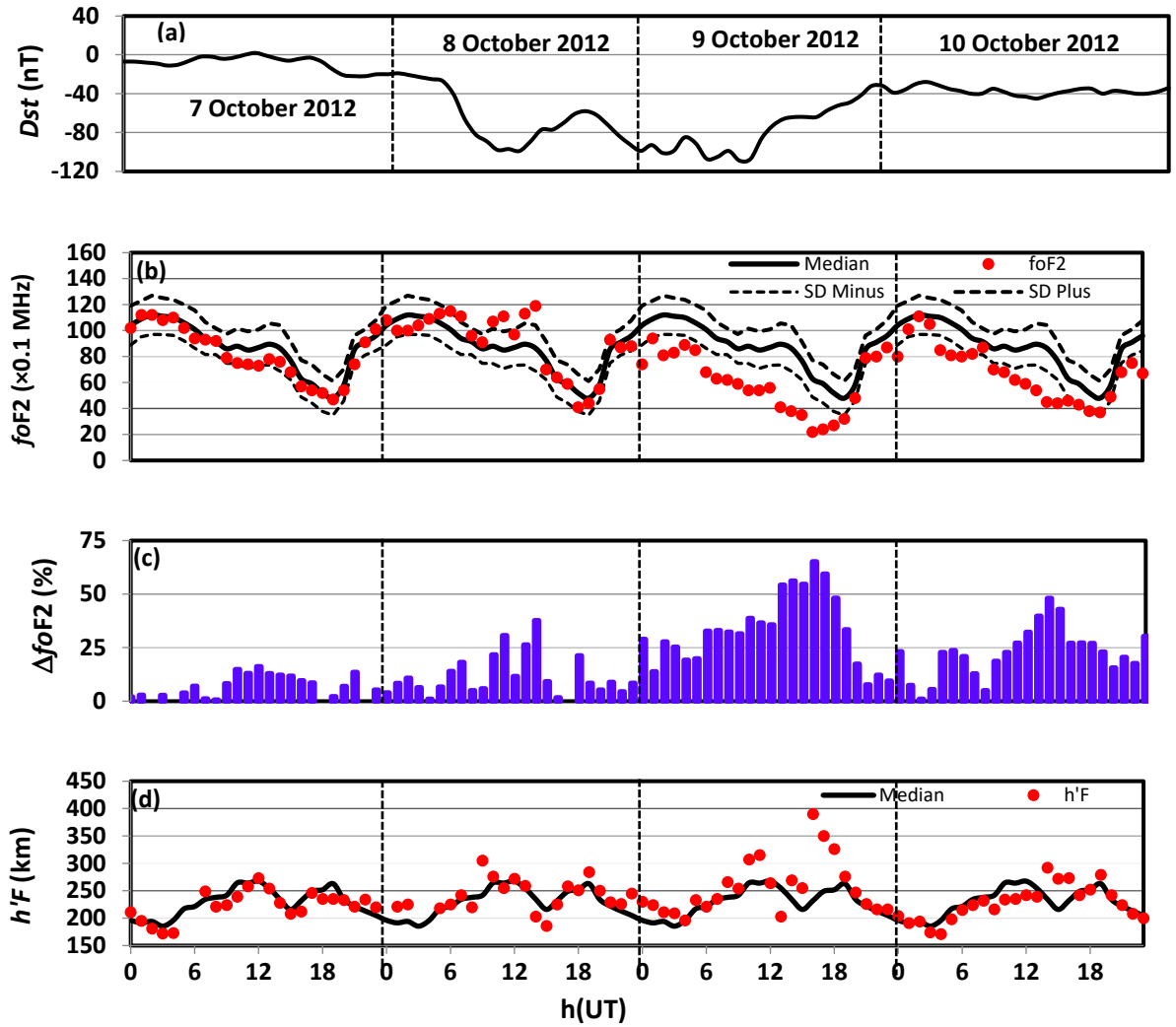

Figure 5. Variations of (**a**) *Dst* index *for* the geomagnetic storm, (**b**) hourly values of critical frequency of F_2 layer (*fo*F2) (MHz $\times$ 10^{-1}), (**c**) Δ*fo*F2%, and (**d**) virtual height of F layer ($h'F$) during 7–10 October 2012 at Townsville station. The median values of *fo*F2 and $h'F$ parameters are shown by solid black curves in panels (**b**,**d**). Dashed curves in panel (**b**) show the variation of *fo*F2 by $\pm$ 1 σ.

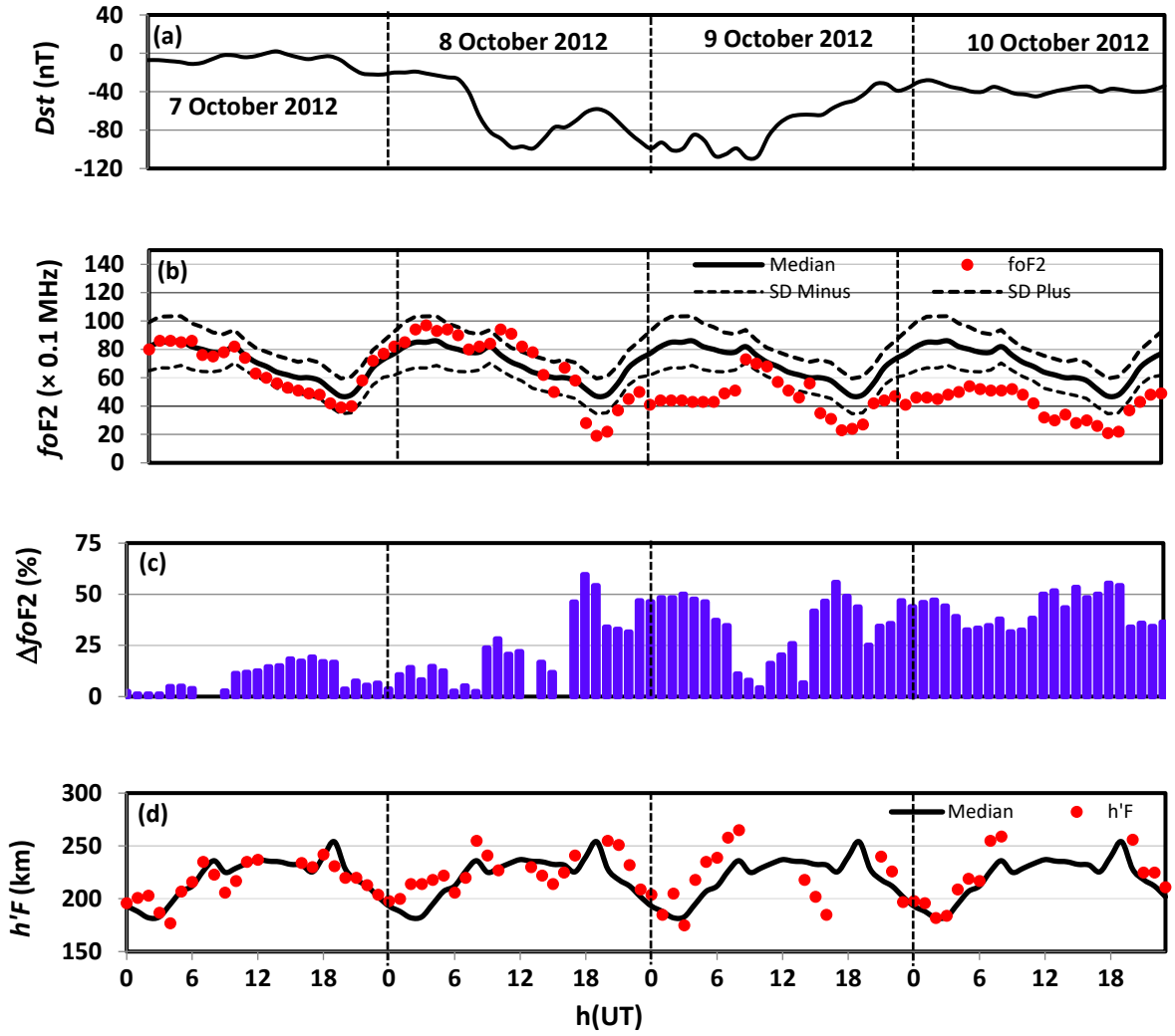

Figure 6. Variations of (**a**) *Dst* index *for* the geomagnetic storm, (**b**) hourly values of critical frequency of F_2 layer (*fo*F2) (MHz $\times$ 10^{-1}), (**c**) Δ*fo*F2%, and (**d**) virtual height of F layer ($h'F$) during 7–10 October 2012 at Canberra station. The median values of *fo*F2 and $h'F$ parameters are shown by solid black curves in panels (**b**,**d**). The dashed curves in panel (**b**) show the variation of *fo*F2 by $\pm$ 1 σ.

The monthly median values of *fo*F2 for 24 h of the day (0–23 h) were calculated excluding the five geomagnetically most disturbed days of the respective month and then the percentage deviation of storm-time *fo*F2 (Δ*fo*F2%) values from the median values were determined using:

$$\Delta foF2\% = \frac{foF2_{storm} - foF2_{median}}{foF2_{median}} \times 100 \quad (1)$$

3. Results

A total of six intense geomagnetic storms during 2012 were examined for any the storm-time variations in the *fo*F2 at low-latitude station, Darwin (Geomagnetic coordinates, 21.96° S, 202.84° E), a low-mid-latitude station, Townsville (28.95° S, 220.72° E) and a mid-latitude station, Canberra (45.65° S, 226.30° E), in the Australian Region. The local time of stations is given as follows: LT (Darwin) = UT + 8.7 h, LT (Townsville) = UT + 9.8 h and LT (Canberra) = UT + 9.9 h. The analysis of storms of 30 September–3 October (minimum *Dst* = $-$122 nT), and 7–10 October (minimum *Dst* = $-$109 nT) was presented as case studies for which $h'F$ data were also utilized. Looking at *fo*F2 variation before and after the storm, a limit of $\pm$1σ (standard deviation) was used to show its day-to-day variability (Figures 1–6).

3.1. Ionospheric Response to the Storm of 30 September to 3 October 2012

The sudden storm commencement (SSC) of the 30 September to 3 October storm occurred at 1300 UT, on 30 September. This storm developed in two steps with the first step having a minimum *Dst* index of −39 nT at 2000 UT and the second step (main phase) with a minimum *Dst* index of −122 nT at 0400 UT on 1 October, as shown in panel a of Figures 1–3. Variations in the *fo*F2, Δ*fo*F2%, and $h'F$ for this storm at three stations are shown in Figures 1–3, respectively. Figure 1b (Darwin station) showed a sharp increase in the *fo*F2 for 4–5 h, with a maximum increase from the median value of 12.6 to 17.1 MHz at 0500 UT, on 1 October giving Δ*fo*F2% of +35.7% (Figure 1c). The *fo*F2 values available online are with scaling up by a factor of 10, so the values shown here are scaled down by a factor of 10 (MHz × 10^{-1}) (also shown in y-axis of panel b) to indicate the actual values. As shown in Figure 1d, to this positive effect in *fo*F2, $h'F$ showed no significant change during the storm main phase, but an increase in the $h'F$ between the SSC and main phase of the storm from 240 to 297 km occurred at 1900 UT on 30 September. The *fo*F2 and $h'F$ variations approached the median value around 0800–0900 UT on 1 October. Thereafter, during the recovery phase of the storm *fo*F2 decreased from 1400–2100 UT on 1 and 2 October and this decrease was accompanied by an increase in the $h'F$ with a maximum decrease from 242 to 319 km at 2000 UT on 2 October. At Townsville station (Figure 2b), the *fo*F2 variation during the main phase of the storm showed an increase (maximum, 10.0–13.3 MHz, at 0600 UT) during 0200–0700 UT on 1 October. Together with the increase in *fo*F2 of about 33% as shown in Figure 2d, there was a short duration increase in the h'F on 1 October. On 1 October between 0900–1000 UT, the *fo*F2 and $h'F$ approached median values showing the storm effect for about 6 h. A decrease in the *fo*F2 from median was observed during 1300–1900 UT, on 1 October, with a simultaneous increase in the $h'F$ with a maximum of about 24%. Another decrease in the *fo*F2 occurred from 0800–2000 UT on 2 October, which was accompanied by an increase in the $h'F$ (maximum, 264–326 km, at 1900 UT). As shown in Figure 3b–d, at Canberra station this particular storm produced an increase in *fo*F2 (maximum 8.0–11.7 MHz at 0500 UT) from 2100 UT on 3 September to 0600 UT on 1 October (about 9 h) with a maximum Δ*fo*F2% of +45.3% (Figure 3c) at 0500 UT on 1 October relative to the median value. There was no significant change in the h'F (Figure 3d) during the increase in *fo*F2. As *fo*F2 approached the median value at around 0800–0900 UT on 1 October during the recovery phase of the storm, a large and long duration decrease in the *fo*F2 was observed (Figure 3b) with a maximum Δ*fo*F2% of −63.5% at 1600 UT on 1 October. This decrease in the *fo*F2 occurred between 1200–2000 UT on 1 October–2 October giving a long duration negative ionospheric storm. This storm produced positive/negative ionospheric effects during its main/recovery phase. Both positive and negative ionospheric storms at Canberra station were stronger and of longer duration as compared to Townsville and Darwin stations showing latitude dependence of the geomagnetic storm effect.

3.2. Ionospheric Response to the Storm of 7–9 October 2012

This geomagnetic storm occurred on 8 October with SSC at about 1700 UT on 7 October and its main phase occurred in multiple steps. As shown in Figure 4a, the *Dst* index decreased to a minimum value of −99 nT at 1200 UT on 8 October and then recovered and then again decreased and recovered in three consecutive steps and had a minimum value of −109 nT at 0800 UT on 9 October. Variations in the *fo*F2, Δ*fo*F2%, and $h'F$ for three stations under this storm are shown in Figures 4–6, respectively. As shown in Figure 4b,d (Darwin station), the *fo*F2 and h'F variations showed no significant change during the first and second steps of the storm development. There occurred a decrease in *fo*F2 during 0200–2000 UT on 9 October with a maximum decrease in *fo*F2 of 7.3–2.8 MHz, at 1600 UT with Δ*fo*F2% of −61.6%. During this period, there was a considerable increase in $h'F$ (maximum 237–331 km 1700 UT) on 9 October. Another decrease in *fo*F2 occurred from 1100–2100 UT on 10 October with a maximum Δ*fo*F2% of about −47%, which was accompanied by a sharp increase in h'F. Figure 5b,d presents the *fo*F2 and $h'F$ variations at Townsville station which during the main phase development of the storm showed a

slight increase in *fo*F2 during 0900–1400 UT on 8 October. There was no significant change in $h'F$ during this first step development of the main phase of the storm. Thereafter, on 9 October, *fo*F2 showed a strong and long duration decrease between 0000–2000 UT, with a maximum decrease from 6.3 to 2.2 MHz (ΔfoF2% of −65.1%) at 1600 UT. The simultaneous strong increase in $h'F$ (maximum 232–390 km at 1600 UT) was found with a maximum of about 68% from the median value. Another event of a decrease in *fo*F2 occurred between 0400–2300 UT on 10 October, which was accompanied by a small increase in $h'F$ (maximum, 216–272 km, at 1500 UT). As shown in Figure 6b–d, Canberra station during the first step development of the main phase showed a small increase in *fo*F2 (maximum 7.1–9.1 MHz at 1000 UT) on 8 October, which had a ΔfoF2% of +28% relative to the median value. The *fo*F2 approached medium value at 1300 UT on 8 October, following which a long duration large decrease in *fo*F2 from 1400 UT on 8 October to 0700 UT on 9 October was observed (Figure 6b) during the second step development of the storm and beyond the recovery phase of the storm with a maximum ΔfoF2% of −59.6% at 1800 UT on 8 October. The *fo*F2 remained below the median value for most of 9–10 October (Figure 6c) showing a long duration of the negative ionospheric storm at Canberra during the storm recovery phase. Increases occurred in $h'F$ during the storm development and recovery phase of the storm during changes in the *fo*F2, as can be seen from Figure 6d.

Table 1 summarizes the *Dst* and *AE* indices and southward IMF B_Z and its duration during the main phase of the storms and *fo*F2 response during the main phases of the six intense geomagnetic storms of 2012 at three different stations in the Southern hemisphere (Australian Region). IMF B_Z varied approximately between −15 to −20 nT for 10 to 20 h duration with an unusually high duration of about 31 h for the 14–15 July storm. The geomagnetic storms of 14–15 July and 30 September–3 October produced positive ionospheric storms at all three stations. The geomagnetic storms of 7–9 October and 13–14 November produced the positive ionospheric storm at Townville and Canberra stations with no effect at Darwin station. The geomagnetic storms of 8–9 March produced the positive ionospheric storm at Canberra with no effect at Townville and Darwin stations. The positive ionospheric storms were not very strong with ΔfoF2% varying between 25 to 40%. The storm of 23–24 April did not produce any effect at any of the three stations.

Table 2 presents ionospheric response during the recovery phase for six intense geomagnetic storms at Darwin, Townsville, and Canberra stations. An increase and a decrease in *fo*F2 signify the positive and negative ionospheric storms, respectively. The negative ionospheric storms were more pronounced compared to positive ionospheric storms and were of longer duration as shown for examples in Figures 1–6 for 30 September to 3 October and 7–10 October storms. Similar long duration negative ionospheric storm was shown by 13–14 November geomagnetic storms at all three stations. The positive ionospheric storms occurred due to the 8–9 March storm and 14–15 July storm (except at Canberra) with a maximum ΔfoF2% of about + 231% for the July storm at the Darwin station. The storm of 7–10 October produced a strong negative ionospheric storm at all three stations with a maximum ΔfoF2% of −65.1% at Townsville. The storm of 23–24 April produced no effect at any of the three stations. A comparison of Tables 1 and 2 shows that during the main phase of the geomagnetic storms, the positive ionospheric storms occurred while during the recovery phase both positive and negative ionospheric storms occurred. The negative ionospheric storms, in general, were stronger and of longer durations (e.g., Figures 1–6) as compared to positive ionospheric storms.

Table 2. Summary of the ionospheric response during the recovery phase for six intense geomagnetic storms at Darwin, Townsville, and Canberra stations during 2012. For the detailed variation of *fo*F2 at Darwin and Canberra stations during 14–15 July storm, the reader is referred to the paper by Kumar and Kumar [7].

Storm	Darwin		Townsville		Canberra	
	***fo*F2**	**Δ*fo*F2 (%)**	***fo*F2**	**Δ*fo*F2 (%)**	***fo*F2**	**Δ*fo*F2 (%)**
8–9 March	Increase	+42.5	Increase	+55.9	Increase	+50.0
23–24 April	No change	—	No change	—	No change	—
14–15 July	Increase	+230.8	Increase	+62.5	Decrease	−48.6
30 September–3 October	Decrease	−42.6	Decrease	−39.2	Decrease	−63.5
7–9 October	Decrease	−61.6	Decrease	−65.1	Decrease	−59.6
13–14 November	Decrease	−20.2	Decrease	−36.8	Decrease	−40.7

4. Discussion

The ionospheric response using the critical frequency of F_2-region (*fo*F2) to six intense geomagnetic storms at a low latitude (Darwin) and a low-mid latitude (Townsville), and a mid-latitude (Canberra) showed the positive storm effect (positive ionospheric storm) during the main phase of the storms and both positive and negative storm effects (negative ionospheric storms) during the recovery phase of the five storms. The storm of 23–24 April did not produce any ionospheric effect. The negative ionospheric storms were stronger and of much longer duration compared to positive ionospheric storms. Generally, a geomagnetic storm is categorized by its SSC, minimum *Dst* (storm intensity), main, and recovery phases. The change in the quiet ionospheric electric field plays a major role in the occurrence of ionospheric storms at the low and mid-latitudes. On quiet conditions (normal days), the equatorial ionospheric electric field is eastward during the daytime and westward at nighttime [18], so the quiet-time ionospheric $\mathbf{E} \times \mathbf{B}$ drifts are upward in the daytime and downward at the nighttime. The normal pattern of $\mathbf{E} \times \mathbf{B}$ drifts can be seriously affected or even reversed by the storm-time prompt penetration of electric fields, PPEFs [13], the disturbance dynamo electric fields, DDEFs [20,21] of high-latitude origin, and overshielding electric field [12,22–24]. The storm-time substorms can also induce both eastward/westward PPEFs under the steady southward/northward Z-component of the interplanetary magnetic field (IMF B_z) conditions [25]. The PPEFs are the potential sources of the positive ionospheric storms (increase in *fo*F2) during the main phases of the five storms (excluding the April storm), as shown in Table 1. This is supported by the fact that the main phase of these storms occurred in the local daytime of the stations when the quiet time ionospheric electric fields are eastward hence the $\mathbf{E} \times \mathbf{B}$ drifts are upward. The main phases of these storms were associated with strong (<-5 nT) southward Z-components of IMF B_Z giving rise to eastward PPEFs which would have enhanced the daytime vertical $\mathbf{E} \times \mathbf{B}$ drifts and strengthened the equatorial plasma fountain [5,18]. The storm of 8–9 March produced a positive ionospheric storm only at mid-latitude station (Canberra) with no effect at Darwin and Townsville stations, indicating that PPEFs did not propagate to the lower latitudes of these two stations. The storms of 7–8 October and 13–14 November produced positive ionospheric storms at the mid-latitude station (Canberra) and the low-mid-latitude station (Townsville) with no effect at Darwin indicating that PPEFs did not propagate to the low latitude of Darwin station. In general, the positive ionospheric effects were stronger at mid-latitude station as compared to low- and low-mid-latitude stations which support the latitudinal dependence of the geomagnetic storm effect. Balan et al. [5] have also reported that during the main phase of geomagnetic storms the daytime eastward PPEFs could be the main driving factors of a positive storm at low and mid-latitudes.

Bagiya et al. [10] reported that the DDEFs caused by the enhanced energy deposited at the high latitudes can perturb the low-latitude ionosphere for one to two days after the main phase of the geomagnetic storm. DDEFs are always opposite to quiet time ionospheric electric fields for both day and night, that is, DDEFs are westward (eastward)

during dayside (nightside) and produce ionospheric effects during the recovery phase of the storms. During the recovery phase, 8–9 March storm showed positive ionospheric storm at all three stations and interestingly 14–15 July storm showed a positive ionospheric storm at Darwin and Townville stations and delayed negative ionospheric storm at the mid-latitude station, Canberra. Kumar and Kumar [7] have studied and discussed the effects of 14–15 July ionospheric effects in the southern hemisphere including at the Darwin and Canberra stations. The positive ionospheric storm during the March geomagnetic storm occurred at the local nighttime of the stations when the quiet-time ionospheric electric field is westward and $\mathbf{E} \times \mathbf{B}$ drifts are downward. The positive ionospheric effect during the March geomagnetic storm accounted for the dominant effect of nighttime DDEFs which would change the normal downward ionospheric drifts or even reverse to the upward direction and hence produce an increase in the electron density or *fo*F2 as occurred at Darwin and Townville during their local nighttime. However, in Canberra, the negative ionospheric storm due to July geomagnetic storm occurred during its local daytime (06–20 LT) and accounted for the combined effects of the westwards DDEFs during local daytime which would reduce the normal upward ionospheric drifts and for equatorward storm-time motion of the thermospheric neutral winds with decreased O/N_2 density ratio due to upwelling of gas with reduced O/N_2 ratio at high latitude moving toward the low latitudes. A long duration decrease in *fo*F2 was found for geomagnetic storms of 30 September–3 October (Figures 1–3), 7–8 October (Figures 4–6), and 13–14 November storms during their recovery phases. The mid-latitude station (Canberra) for these storms showed the longest duration of negative ionospheric storms and least by the Darwin station (e.g., Figures 1–6). These negative ionospheric storms are accounted for combined effects DDEFs and equatorward storm-time thermospheric neutral winds with decreased O/N_2 density ratio due to upwelling O/N_2 ratio at high latitude moving toward the low latitudes with dominating effect of the latter mechanism. During the recovery phase, the overshielding electric field would also have contributed to the ionospheric effects during these storms by instantly imposing additional ionospheric zonal electric fields in the opposite directions in dayside and nightside, respectively [12]. The contribution of the overshielding electric field would be stronger for the 30 September–3 October and 7–10 October storms which had a stronger (5 to 10 nT) northward component of IMF B_Z during their recovery phases as compared to the other four storms that had a week northward component of IMF B_Z which was mostly southward with weak intensity. The northward turning of the IMF *Bz* marks dominance of the overshielding field which penetrates in a few seconds from high latitudes down to low/equatorial latitudes and can occur both for short and long periods [12,23]. The strength (Table 2) and durations (e.g., Figures 1–6) of ionospheric storms clearly show the latitude dependent effect of these mechanisms (undershielding PPEFs, DDEFs, overshielding field, and storm-induced circulation) with maximum effect at the mid-latitude station (Canberra) which needs further investigation.

During intense geomagnetic storms, the high-latitude Joule heating (JH) could persist from a few hours to several days which raises the temperature of the upper thermosphere and generates large scale atmospheric gravity waves (AGWs) with a phase speed of about 600 m s^{-1} [26]. AGWs launched from the auroral regions due to JH propagate toward equatorial latitudes. At the ionospheric height, AGWs generate traveling ionospheric disturbances (TIDs) [5] via the neutral–plasma interaction and are identified by wave-like fluctuations in the ionospheric parameters [27]. TIDs can also contribute to the changes in *fo*F2 during the main phase of the storm indicated by the high value of the *AE* index during these storms (Table 1). The JH also drives equatorward storm-time thermospheric neutral winds with decreased O/N_2 density ratio due to upwelling of this gas at high latitude moving toward the low latitudes [28,29] and downwelling of gas with reduced O/N_2 ratio at low latitudes. In our study high values of the *AE* index associated with these storms (Table 1) show the reasonably high *JH*. The *JH* and *AE* indices are linearly related as $JH = 0.19\ AE$ [30] and $JH = 0.33\ AE$ [31] where *JH* is in gigawatts and *AE* in

nanotesla. This *JH* would result in a negative ionospheric storm (decrease in *fo*F2) during the recovery phase of storm at mid and low-latitude stations due to composition changes that occur due to an equatorward geomagnetic storm-induced circulation of gas with a depleted O/N_2 ratio. At the ionospheric height, Balan et al. [5] also studied the physical mechanisms of the ionospheric storms during the recovery phase of geomagnetic storms using CHAMP Ne, GPS–TEC data, and the Sheffield University plasmasphere ionosphere model, and reported that storm-time equatorward neutral wind could be the major cause of ionospheric effects. The AGWs are launched from the auroral regions due to JH and propagate toward equatorial latitudes producing TIDs. Variation in the ionospheric electron density is because of the enhanced JH caused by the auroral electrojet current, where the energy is transported to the equatorial region with a delay of 24 h [10,32]. Kumar and Kumar [7] found a strong long-duration decrease in the *fo*F2 during the recovery phase of the St. Patrick's Day storms in March 2012, 2013, and 2015 in the southern hemisphere. They based on the thermospheric O/N_2 density data measured by the global ultraviolet imager (GUVI) onboard the thermosphere, ionosphere, mesosphere energetics, and dynamics (TIMED) satellite accounted decrease in *fo*F2 to the decrease in thermospheric O/N_2 density ratio at lower latitudes and partly due to DDEFs. Habarulema et al. [32] studied TIDs by measuring TEC derived from the global navigational satellite system and radio occultation during the same storms that we have studied here for the geographic latitudinal coverage of 10–40° S within a longitude sector of 10–40° E. A common result portrayed to all storms was the presence of large scales TIDs during the storm main phases. Authors [32] confirmed that equatorward large-scale TIDs were always observed and may have contributed to the positive storm effects (in five cases) in the midlatitudes (10–40° S as considered by [32]). This has implications to our findings, at least for positive ionospheric storms observed during the main phase of five out of six intense geomagnetic storms. The variability of ionospheric effects (Tables 1 and 2) of intense geomagnetic storms of this study is attributed to the ionospheric variability at different scales (e.g., day-to-day, seasonal, 27 day), variability of storm-time mechanisms, and upward coupling of meteorologically generated AGWs and atmospheric waves and tides from the lower to the upper atmosphere (e.g., [33–36]) which is a subject of a separate study.

5. Conclusions

In this paper, the ionospheric response is studied by analyzing *fo*F2 variation at Darwin, Townsville, and Canberra stations in the Australian region during the six intense geomagnetic storms (-100 nT $\leq Dst \geq -200$ nT) that occurred during 2012. The main results of the investigation are concluded as:

- Positive and negative storm effects (ionospheric storms) in *fo*F2 were observed during five out of six intense storms at both low and mid-latitudes stations. The storms of which the main phase occurred in the local daytime showed only positive ionospheric storms during their main phases associated with eastward PPEFs which strengthened the equatorial plasma fountain by enhancing the $\mathbf{E} \times \mathbf{B}$ vertical plasma drifts;
- The recovery phase of the storms showed both positive and negative ionospheric storms with the predominant occurrence of negative ionospheric storms which were stronger and of long duration as compared to positive ionospheric storms;
- Long duration decreases in *fo*F2 (negative ionospheric storms) during the recovery phase of storms are related DDEFs and overshielding electric field which changed the normal ionospheric $\mathbf{E} \times \mathbf{B}$ drifts and to the equatorward motion of storm-time thermospheric neutral winds with decreased O/N_2 density ratio.

Further work on long-term data analysis over the varying longitudinally located stations in the low- to mid-latitude region is required for a better understanding of the F_2-region response to the geomagnetic storms.

Supplementary Materials: The following supporting information can be downloaded at: https://www.mdpi.com/article/10.3390/atmos13030480/s1, Figure S1: The IMF B_Z variations during the magnetic storms given in Table 1.

Author Contributions: Conceptualization, S.K. and E.A.K.; methodology, S.K. and E.A.K.; resources, E.A.K. and S.K.; formal analysis, E.A.K.; writing—original draft, E.A.K. and S.K.; writing—review and editing, S.K.; visualization, S.K. All authors have read and agreed to the published version of the manuscript.

Funding: This research received no external funding.

Institutional Review Board Statement: Not applicable.

Informed Consent Statement: Not applicable.

Data Availability Statement: Not applicable.

Acknowledgments: The *fo*F2 data were obtained from the World Data Centre, Bureau of Meteorology, Australia (online at http://www.sws.bom.gov.au/World_Data_Centre, accessed on 22 December 2021). The *Dst* index data were obtained from the World Data Centre, Kyoto University, Kyoto, Japan (online at http://www.ssde.u-kigi-kyoto-ac.jp, accessed on 22 December 2021).

Conflicts of Interest: The authors declare no conflict of interest.

References

1. Chen, Y.; Liu, L.; Le, H.; Wan, W. Geomagnetic activity effect on the global ionosphere during the 2007–2009 deep solar minimum. *J. Geophys. Res. Space Phys.* **2014**, *119*, 3747–3754. [CrossRef]
2. Danilov, A. Ionospheric F-region response to geomagnetic disturbances. *Adv. Space Res.* **2013**, *52*, 343–366. [CrossRef]
3. Kumar, S.; Kumar, A.; Menk, F.; Maurya, A.K.; Singh, R.; Veenadhari, B. Response of the low-latitude D region ionosphere to extreme space weather event of 14–16 December 2006. *J. Geophys. Res. Space Phys.* **2015**, *120*, 788–799. [CrossRef]
4. Kumar, S.; Kumar, S.R. Equatorial ionospheric TEC and scintillations under the space weather events of 4–9 September 2017: M-class solar flares and a G4 geomagnetic storm. *J. Atmos. Sol.-Terr. Phys.* **2020**, *209*, 105421. [CrossRef]
5. Balan, N.; Otsuka, Y.; Nishioka, M.; Liu, J.; Bailey, G. Physical mechanisms of the ionospheric storms at equatorial and higher latitudes during the recovery phase of geomagnetic storms. *J. Geophys. Res. Atmos.* **2013**, *118*, 2660–2669. [CrossRef]
6. Sahai, Y.; Fagundes, P.; Becker-Guedes, F.; Bolzan, M.; Abalde, J.; Pillat, V.; De Jesus, R.; Lima, W.; Crowley, G.; Shiokawa, K. Effects of the major geomagnetic storms of October 2003 on the equatorial and low-latitude F region in two longitudinal sectors. *J. Geophys. Res. Space Phys.* **2005**, *110*. [CrossRef]
7. Kumar, S.; Kumar, V.V. Ionospheric response to the St. Patrick's Day space weather events in March 2012, 2013, and 2015 at southern low and middle latitudes. *J. Geophys. Res. Space Phys.* **2019**, *124*, 584–602. [CrossRef]
8. Huang, C.-S.; Zhang, Y. Equatorial plasma drifts during the magnetic storm on November 7–11, 2004: Identifications of the roles of penetration and disturbance dynamo electric fields with multi instrumental measurements. *J. Geophys. Res. Space Phys.* **2021**, *126*, e2021JA029386. [CrossRef]
9. Kuai, J.; Liu, L.; Liu, J.; Zhao, B.; Chen, Y.; Le, H.; Wan, W. The long-duration positive storm effects in the equatorial ionosphere over Jicamarca. *J. Geophys. Res. Space Phys.* **2015**, *120*, 1311–1324. [CrossRef]
10. Bagiya, M.S.; Iyer, K.N.; Joshi, H.; Thampi, S.V.; Tsugawa, T.; Ravindran, S.; Sridharan, R.; Pathan, B.M. Low-latitude ionospheric-thermospheric response to storm time electrodynamical coupling between high and low latitudes. *J. Geophys. Res. Space Phys.* **2011**, *116*, A01303. [CrossRef]
11. Huang, C. Disturbance dynamo electric fields in response to geomagnetic storms occurring at different universal times. *J. Geophys. Res. Space Phys.* **2013**, *118*, 496–501. [CrossRef]
12. Hui, D.; Vichare, G. Variable responses of equatorial ionosphere during undershielding and overshielding conditions. *J. Geophys. Res. Space Phys.* **2019**, *124*, 1328–1342. [CrossRef]
13. Huang, C.-S.; Foster, J.C.; Kelley, M.C. Long-duration penetration of the interplanetary electric field to the low-latitude ionosphere during the main phase of magnetic storms. *J. Geophys. Res.* **2005**, *110*, A11309. [CrossRef]
14. Huang, C.-S.; Rich, F.J.; Burke, W.J. Storm time electric fields in the equatorial ionosphere observed near the dusk meridian. *J. Geophys. Res. Space Phys.* **2010**, *115*, A08313. [CrossRef]
15. Lu, G.; Hagan, M.; Häusler, K.; Doornbos, E.; Bruinsma, S.; Anderson, B.; Korth, H. Global ionospheric and thermospheric response to the 5 April 2010 geomagnetic storm: An integrated data-model investigation. *J. Geophys. Res. Space Phys.* **2014**, *119*. [CrossRef]
16. Uma, G.; Brahmanandam, P.; Kakinami, Y.; Dmitriev, A.; Devi, N.L.; Kiran, K.U.; Prasad, D.; Rao, P.R.; Niranjan, K.; Babu, C.S. Ionospheric responses to two large geomagnetic storms over Japanese and Indian longitude sectors. *J. Atmos. Sol.-Terr. Phys.* **2012**, *74*, 94–110. [CrossRef]

17. Wang, C.; Zhang, Q.; Chi, P.; Li, C. Simultaneous observations of plasmaspheric and ionospheric variations during magnetic storms in 2011: First result from Chinese Meridian Project. *J. Geophys. Res. Space Phys.* **2013**, *118*, 99–104. [CrossRef]
18. Kumar, S. F2-region response to geomagnetic storms at the equatorial anomaly during 1989–2001. *Phys. Scr.* **2005**, *72*, 100. [CrossRef]
19. Rawat, R.; Alex, S.; Lakhina, G. Storm-time characteristics of intense geomagnetic storms at low-latitudes and associated energetics. *J. Atmos. Sol.-Terr. Phys.* **2010**, *72*, 1364–1371. [CrossRef]
20. Blanc, M.; Richmond, A.D. The ionospheric disturbance dynamo. *J. Geophys. Res.* **1980**, *85*, 1669–1686. [CrossRef]
21. Fejer, B.G.; Larsen, M.F.; Farley, D.T. Equatorial disturbance dynamo electric fields. *Geophy. Res. Lett.* **1983**, *10*, 537–540. [CrossRef]
22. Kikuchi, T.; Ebihara, Y.; Hashimoto, K.K.; Kataoka, R.; Hori, T.; Watari, S.; Nishitani, N. Penetration of the convection and overshielding electric fields to the equatorial ionosphere during a quasiperiodic DP 2 geomagnetic fluctuation event. *J. Geophys. Res.* **2010**, *115*, A05209. [CrossRef]
23. Kobéa, A.T.; Richmond, A.D.; Emery, B.A.; Peymirat, C.; Luhr, H.; Moretto, T.; Hairston, M.; Amory-Mazaudier, C. Electrodynamic Coupling of High and Low latitudes Observations on May 27, 1993. *J. Geophys. Res.* **2000**, *105*, 22979–22989. [CrossRef]
24. Peymirat, C.; Richmond, A.D.; Kobea, A.T. Electrodynamic coupling of high and low latitudes: Simulations of shielding and overshielding effects. *J. Geophys. Res.* **2000**, *105*, 22991–23003. [CrossRef]
25. Hui, D.; Chakrabarty, D.; Sekar, R.; Reeves, G.D.; Yoshikawa, A.; Shiokawa, K. Contribution of storm time substorms to the prompt electric field disturbances in the equatorial ionosphere. *J. Geophys. Res. Space Phys.* **2017**, *122*, 5568–5578. [CrossRef]
26. Fuller-Rowell, T.J.; Codrescu, M.V.; Moffett, R.J.; Quegan, S.S. Response of the thermosphere and ionosphere to geomagnetic storms. *J. Geophys. Res.* **1994**, *99*, 3893–3914. [CrossRef]
27. Miyoshi, Y.; Jin, H.; Fujiwara, H.; Shinagawa, H. Numerical study of traveling ionospheric disturbances generated by an upward propagating gravity wave. *J. Geophys. Res. Space Phys.* **2018**, *123*, 2141–2155. [CrossRef]
28. Prölss, G.W. Ionospheric F-region storms. In *Handbook of Atmospheric Electrodynamics*; Volland, H., Ed.; CRC Press: Boca Raton, FL, USA, 1995; Volume 2, pp. 195–248.
29. Bolaji, O.S.; Fashae, J.B.; Adebiyi, S.J.; Owolabi, C.; Adebesin, B.O.; Kaka, R.O.; Ibanga, J.; Abass, M.; Akinola, O.O.; Adekoya, B.J.; et al. Storm time effects on latitudinal distribution of ionospheric TEC in the American and Asian-Australian sectors: August 25–26, 2018 geomagnetic storm. *J. Geophys. Res. Space Phys.* **2021**, *126*, e2020JA029068. [CrossRef]
30. Baumjohann, W.; Kamide, Y. Hemispherical Joule heating and the AE indices. *J. Geophys. Res.* **1984**, *89*, 383–388. [CrossRef]
31. Ahn, B.-H.; Akasofu, S.-I.; Kamide, Y. The Joule heat production rate and the particle energy injection rate as a function of the geomagnetic indices AE and AL. *J. Geophys. Res.* **1983**, *88*, 6275–6287. [CrossRef]
32. Habarulema, J.B.; Katamzi, Z.T.; Sibanda, P.; Matamba, T.M. Assessing ionospheric response during some strong storms in solar cycle 24 using various data sources. *J. Geophys. Res. Space Phys.* **2017**, *122*, 1064–1082. [CrossRef]
33. Rishbeth, H.; Mendillo, M. Patterns of ionospheric variability. *J. Atmos. Sol. Terr. Phys.* **2001**, *63*, 1661–1680. [CrossRef]
34. Mendillo, M. *Chapter 2: Day-to-Day Variability of the Ionosphere, Dynamical Ionosphere a Systems Approach to Ionospheric Irregularity*; Elsevier: Amsterdam, The Netherlands, 2020.
35. Chen, Z.; Wang, J.S.; Deng, X.; Deng, Y.; Huang, C.M.; Li, H.M.; Wu, Z.X. Study on the relationship between the residual 27 day quasi periodicity and ionospheric Q disturbances. *J. Geophys. Res. Space Phys.* **2017**, *122*, 2542–2550. [CrossRef]
36. Fejer, B.G. Low latitude storm time ionospheric electrodynamics. *J. Atmos. Sol.-Terr. Phys.* **2012**, *64*, 1401–1408. [CrossRef]